Geophysical Journal International

Friction and Roughness of a Melting Rock Surface

Journal:	*Geophysical Journal International*
Manuscript ID:	GJI-09-0337.R1
Manuscript Type:	Research Paper
Date Submitted by the Author:	
Complete List of Authors:	Nielsen, Stefan; Istituto Nazionale di Geofisica e Vulcanologia, Sismologia e Tettonofisica Di Toro, Giulio; Università degli studi di Padova, Dipartimento di Geoscienze Griffith, Ashley; Istituto Nazionale di Geofisica e Vulcanologia, Sismologia e Tettonofisica
Keywords:	Friction < COMPOSITION and PHYSICAL PROPERTIES, Earthquake dynamics < SEISMOLOGY, Rheology and friction of fault zones < TECTONOPHYSICS, Dynamics and mechanics of faulting < TECTONOPHYSICS

Friction and roughness of a melting rock surface

February 5, 2010

Stefan B. Nielsen[1], Giulio Di Toro[1,2], W. Ashley Griffith[1, 3]

Abstract

Under extreme conditions like those encountered during earthquake slip, frictional melt is likely to occur. It has been observed on ancient faults that the melt is mostly extruded toward local extensional jogs or lateral tension cracks. In the case of laboratory experiments with a rotary shear apparatus, melt is extruded from the sample borders. When this happens, a thin and irregular melt layer is formed whereby the normal load is still in part supported by contact asperities under an incipient yield condition (as in dry friction models), but also, in the interstices between asperities, by the pressure of the viscous fluid wetting the interface. In addition, roughness of the surface is dynamically reshaped by the melting process of an inhomogeneous material (polymineral rock). In particular, we argue that the roughness of the melting surface decreases with melting rate and temperature gradient perpendicular to the fault. Taking into account the above conditions, we obtain an expression for the average melt layer thickness and viscous pressure that may be used in estimates of friction in the presence of melt. We argue that the ratio of melt thickness to roughness depends on sliding velocity; such a ratio may be used as a gauge of slip-rate during fossil earthquakes on faults bearing pseudotachylite (solidified melt). Finally, we derive an improved analytical solution for friction in the presence of melt including the effect of roughness evolution.

[1]Istituto Nazionale di Geofisica e Vulcanologia, Roma, Italy
[2]Dpto. di Geoscienze, Università degli studi di Padova, Italy
[3]Now at Department of Geology and Environmental Science, University of Akron, USA.

Introduction

0.1 Earthquake rupture is essentially controlled by the dynamics of friction of rock surfaces under rapid slip on faults buried at several km depth. As a consequence of the lithostatic and tectonic load, the conditions are rather extreme: normal stress is of the order of tens to hundreds MPa and slip velocities are of the order of the meter per second. The amount of heat produced over time intervals of a few seconds is such that phase transition are rapidly triggered (Jeffreys 1942; Hirono et al., 2007; Rice, 2006; Sulem & Famin, 2009; Hamada et al., 2009) altering the nature and rheology of the fault zone in the vicinity of the sliding surface.

0.2 The above arguments and their implications for earthquake studies have stimulated a rapidly growing body of theoretical, experimental and field investigations on frictional sliding in the presence a number of processes, such as flash heating (Beeler et al., 2008), fluid pressurization (Bizzarri & Cocco, 2006), gelification (Di Toro et al., 2004; Goldsby & Tullis, 2002), decarbonation (Han et al., 2007) , dehydration (Brantut et al., 2008) and melting (Hirose & Shimamoto 2005; Spray, 2005; Di Toro et al., 2006). In the case of melting, it is attested by the presence of pseudotachylite (glassy veins of rapidly solidified melt, Shand 1916) observed on some exhumed ancient faults, and it has been the object of particular attention (Sibson 1975, Di Toro et al., 2006). The present study complements recent investigations on frictional melt (Nielsen et al. 2008), by introducing the effect of surface roughness in relation to normal stress and friction across a viscous melt layer.

0.3 **It is frequently observed in pseudotachylite-bearing, ancient seismic faults that** frictional melts produced during seismic slip in nature are mostly squeezed out from the slipping zone, either injected in the wall rocks or they may pool toward extensional jogs (Sibson, 1975; Di Toro et al., 2005). **[I-1a] As a consequence, many segments of the faults show a very thin remnant layer of solidified melt (a fraction of mm), decorated by sidewards injection veins and separated by locally thicker pools at extensional jogs. The effective thickness of melt within the fault vein is rather small, though a larger average thickness (total melt volume produced per unit fault area) may result when including pools and lateral vein injections (Di Toro et al., 2005).**

0.4 In high velocity rotary shear experiments, frictional melt is reproduced under dry ambient conditions when samples of silicate rocks are forced to slide against each other at

seismic slip rates ($\approx 1\,\mathrm{m/s}$) under an intermediate (1-20 MPa) applied normal stress (Tsutsumi & Shimamoto, 1997; Hirose & Shimamoto, 2005; Di Toro et al., 2006; Del Gaudio et al., 2009). In these experiments, shear stress evolves with slip from a value initally high on average, compatible with standard Byerlee rock friction coefficients ($\mu \geq 0.6$), toward a much lower steady-state shear stress, indicative of the presence of a lubrication process on the interface. Melt is extruded from the sample to the open air (Hirose & Shimamoto, 2005; Spray, 1995; Di Toro et al., 2006), **resulting in an effectively sub-millimeter-thin layer of melt also in the case of the these experimentally produced faults.**

[I-4] In the experiments the extrusion is only limited by the viscosity of the melt, because no resistance is opposed to the outflow of the melt at the edges of the sample into the open air (ambient pressure is negligible). On natural faults, we argue that the pressure gradient between the shear layer and the extrusion volume (injection veins and/or extension jogs) is very large, because both injection veins and jogs are caused by opening tension (see, for example Di Toro et al, Nature, 2005), rather that hydrofracturing due to melt overpressure. The resulting pressure in the extrusion volumes is negligible compared to that inside the fault and should not oppose significantly the outflow of melt. As melting proceeds fault slip increases and the opening gaps widen, so that the pressure does not increase in time in the pooling reservoirs. As a result we can reasonably consider that the extrusion rate is controlled by the viscous squeeze, under a pressure gap which is approximately constant and equal to the normal stress σ_n, in a situation similar to the experimental conditions. The distance between a point inside the melt and the nearest extrusion vein may fluctuate during one seismic episode, if slip amount is close or larger than the inter-vein distance; however the average extrusion flow length on a larger fault area should remain the same, keeping the the boundary conditions for melt extrusion stable with respect to the global mass balance.

Following (Lee & Ladd, 2002; Fialko & Khazan, 2005; Nielsen et al., 2008) we assume that if a viscous melt patch of linear dimension R and of thickness 2ω is being squeezed at a rate $2\,\dot{\omega}_c$(convergence rate of two opposite melt layer boundaries), a viscous push in the form

$$\sigma_v = C \;\; \eta_e \, \dot{\omega}_c \, R^2/\omega^3 \tag{1}$$

will develop which resists the convergence of the opposite sliding surface (C is a dimensionless factor depending on the geometry of the contact and η_e an equivalent viscosity for the extrusion of a cross-layer inhomogeneous film of fluid). **In the case of cylindrical symmetry, such as rotary shear experiments, R is the outer radius of the sample, while for faults R can be the average distance between injection veins.** For an irregular surface, melt thickness ω is understood as an average across the contact area. In Nielsen et al. (2008), it was noted that the experimental data showed evidence for an apparent residual stress σ_0, in addition to the viscous push, leading to an empirical normal stress fit of the form:

$$\sigma_n = C \ \ \eta_e \, \dot{\omega}_c \, R^2/\omega^3 + \sigma_0 \tag{2}$$

0.8 As one interpretation of such a residual stress, it was proposed that part of the load is supported by local partial contact of the two solid blocks across the melt layer due to the roughness in the surface topography. **[I-1b] Asperity contact across the melt layer can take place because of the reduced melt thickness both in experimental samples and on natural faults.** In the present study we develop the above concept of partial contact, based on micro-structural descriptions of the interface morphology, and seek a mathematical form for σ_0. We investigate the consequences on the frictional behavior of faults where melting occurs, and derive a link between surface roughness, melt thickness and slip rate. **[I-1b] Although the solidified melt encountered on natural faults is also observed to form locally thicker pools, we believe that the latter are not significantly contributing to the frictional behavior but rather act as passive buffers. As a consequence, the asperity model adopted for this study should apply to frictional melt on both natural and experimental faults.**

0.9 In addition, based on theoretical arguments and a few experimental examples, we show that a combination of measurable parameters (related to the melting surface roughness and to the thickness of the melt) is quantitatively related to the slip rate V. Ideally, this relation could be used as a gage for posthumous estimate of the co-seismic slip rate on faults bearing solidified frictional melt, providing an additional tool to reconstruct earthquake dynamics from fossil markers on ancient seismic faults. In previous studies, field observations already provided constraints on co-seismic friction (Sibson, 1975; Di Toro et al. (2006)) rupture directivity and

rupture propagation velocity (Di Toro et al., 2005) and earthquake energy budget (Pittarello et al., 2008).

1 Hertzian contact

1.10 During slip in the presence of friction melt, most of the removable melt is being squeezed out of the interface and contacting areas start to appear and are continually renewed across the sliding surface. We must analyze the convergence of the two solid boundaries in the framework of Hertzian contact between two rough elastic surfaces, with plastic yield locally occurring at isolated asperity contacts where indentation hardness σ_c of the material is exceeded. **[I-1c] In our case, what we refer to as contact asperities are actually places where the two rocks are still separated by an extremely thin (micron) melt film. The latter is impossible to squeeze out so that the weight is effectively supported across the asperities.** For small slip amounts ($<$ 1 cm) melt is generally scarce or absent and it has been proposed to analyze friction in terms of flash (short lived) heating and weakening of local contact asperities (Beeler et al., 2008). On the other hand, after a few centimeters of slip or more, silicatic rocks under dry conditions, high normal stress and high slip rates, produce a pervasive layer of melt, with a few local asperity contacts across the interface (Hirose & Shimamoto, 2005). This is the case investigated here. To this purpose, we develop some fundamental concepts of tribology regarding the contact of rough surfaces, which we adapt to the case where a fluid pressure (viscous push) is present at the interface.

1.11 Let's rapidly recall a couple of fundamental concepts of tribology regarding the contact of rough surfaces:

1.12 (1) The average spacing between the two rough surfaces does not vary significantly with normal load. Hertzian contact between two isolated, elastic spheres yields an interpenetration distance h varying non-linearly with the normal load in the form $h \propto F^{2/3}$(Landau & Lifshitz, 1975). However, as shown by (Greenwood, 1992; Persson, 2000), assuming that the surface topography of two solids in frictional contact across an area A can be mimicked by adjoining N spherical caps with average radius λ and a given probability distribution of height $\psi(z)$, the separation ω between two rough surfaces under a normal load F follows the equation:

1.13

$$\left(\frac{\omega}{\omega_0}\right)^2 = 2\,\log\left(N\,\omega_0^{3/2}\,\lambda^{1/2}\,\frac{4}{3(1-\nu_P^2)}\,\frac{E}{F}\right) - 5\,\log\left(\frac{\omega}{\omega_0}\right) \qquad (3)$$

where ω_0 is the characteristic elevation of the asperities on the surface, e.g., the rms of the asperity height probability distribution $\psi(z)$ (z being the asperity height with respect to the reference plane $z = 0$ such that $\int_A \psi(z)\,da = 0$), ν_P is the Poisson ratio and E is the Young modulus of the medium. A schematic illustration of the meaning of the ω, ω_0 and λ in the above equation is provided in Fig (1).

1.14 It appears that the separation ω is weakly sensitive to normal load σ_n, resulting for practical purposes in a bounded value $\omega = 2\,\omega_0 \rightarrow 3\,\omega_0$. If we take $\omega_0 \approx 70\,\mu m$, consistent with the observed values on thin sections of fossil fault rocks (Fig. 2a) bearing solidified melt (pseudotachylite), or laboratory samples from frictional melt experiments (Fig. 2b,c), we obtain typically that $140 < \omega < 210\,\mu m$.

1.15 For simplicity, we may approximate the total area as $A \propto N\,\lambda^2$. This assumes that $\frac{1}{N}\sum_{n=1}^{N}\lambda_n^2 = (\frac{1}{N}\sum_{n=1}^{N}\lambda_n)^2 = \lambda^2$, which is acceptable if the radii λ_n are all similar and if the virtual spheres are packed with a reasonably regular spacing along the plane $z = 0$. If the spheres overalp on average of about 22% of their radius, the proportionnality reduces in $A = N\,\pi\,\lambda^2$. Diversely, the proportionnality factor will change without altering substantially the scaling law and the following results. Finally, we may write the normal force as $F = A\,\sigma_n$. As a consequence, we obtain the modified expression:

$$\left(\frac{\omega}{\omega_0}\right)^2 = 2\,\log\left(\frac{4}{3(1-\nu_P^2)}\,\left(\frac{\omega_0}{\lambda}\right)^{3/2}\,\frac{E}{\sigma_n}\right) - 5\,\log\left(\frac{\omega}{\omega_0}\right) \qquad (4)$$

1.16 (2) The area of real contact between two rough surfaces increases proportionally to normal load (Dieterich & Kilgore, 1994). Letting α be the proportion of real contact area vs. total area, it can be shown that $\alpha = \sigma_n/\sigma_c$; the contact asperities are under a compressive stress close to the material strength σ_c, in a state of incipient plastic yield (Dieterich & Kilgore, 1994; Persson, 2000). In our case, contact areas are constituted by those patches where the melt thickness becomes negligible and the two solid sides touch each other. We need to slightly modify the above definition of α as a the ratio of normal to yield stress, due to the presence of the additional pressure generated by extrusion of the viscous melt (viscous push σ_v). We can obtain a modified relationship by simply writing the total load across the area as the sum of

two contributions:

$$\sigma_n = \alpha\,\sigma_c + (1-\alpha)\,\sigma_v \tag{5}$$

Interestingly, an expression similar to (5) is used to account for the presence of pore fluid pressure on faults (Scholz 1990). Using (1) for the viscous push σ_v due to the squeezing of the interface at a rate $\dot{\omega}_c$, we may write:

$$\sigma_n - \alpha\,\sigma_c = (1-\alpha)\,C\,\eta_e\,\dot{\omega}_c\,R^2/\omega^3 \tag{6}$$

1.17 We may derive an independent relationship for α directly from the separation distance of the two boundaries, using (Persson, 2000):

1.18

$$\alpha = \sqrt{\frac{1}{2\,\pi}}\,\frac{\pi\,N\,\lambda}{A}\,\frac{\omega_0^3}{\omega^2}\,\exp\left(-\frac{\omega^2}{2\,\omega_0^2}\right) \tag{7}$$

where A is the total area and N the number of asperities of average radius λ. We may again assume that the total area A scales with the number of N of asperities such that $A \approx N\,\pi\,\lambda^2$ to obtain:

$$\alpha \approx \sqrt{\frac{1}{2\pi}}\,\frac{\omega_0^3}{\omega^2\lambda}\,\exp\left(-\frac{\omega^2}{2\,\omega_0^2}\right) \tag{8}$$

with the constraint that

1.19

$$\alpha \leq \sigma_n/\sigma_c \tag{9}$$

because the total stress cannot exceed the applied normal stress σ_n.

2 Origin of the melting surface roughness: theoretical considerations

2.20 Micro-structural analysis of fault and laboratory samples show that a minimum quantity of melt always remains trapped in the roughness of the boundary surfaces formed by melt. The roughness is determined by a variety of small-scale inhomogeneities of mechanical (e.g., indentation hardness, resistance to wear), structural (e.g., presence of fluid inclusions, cleavage surfaces, micro-fractures), mineralogical (e.g., melting temperature) or **thermo-mechanical**

nature (thermal cracking). The resulting boundary constitutes a strongly uneven and wavy surface (see Fig. 2,3,4) where the topographical fluctuations are of the order of $\omega_0 \approx 50-150\mu$m over distances λ (or asperity radii) of comparable size, though they are found to vary depending on the type of rock, mineral grain size and also on melting conditions (Hirose & Shimamoto, 2003).

2.21 Indeed, it is essential to note that under frictional melting conditions, the nature of surface roughness changes depending on the advancement of slip and on the levels of slip rate and normal stress. As pointed out in Hirose & Shimamoto (2003), the geometry of the irregular melt/solid boundary is conditioned by a number of factors: the selective or "preferential" melting (hydrous minerals tend to melt faster given their lower melting point, e.g., 600^{o}Cfor Biotite compared to 1700^{o}C for Quartz, see Shand, 1916; Spray, 1992); the Gibbs-Thomson effect (i.e. the local melting temperature of a mineral in contact with melt is lowered in proportion to its curvature, tending to eliminate sharp corners in favour of round-shaped melting surfaces); the preferential melting along grain boundaries and cracks; and the indentation, cracking or plastic yielding at solid/solid contacts.

2.22 Here we argue that the evolution of temperature gradient perpendicular ot the fault surface, in the solid next to the melting boundary, will strongly modulate the role of the above factors in shaping the irregular surface, in particular, in the preferential melting of minerals with different composition. A steep temperature gradient will result in 1) a more planar and less irregular surface 2) smaller wavelength fluctuations in the surface topography.

2.23 In order to explain these effects, we take the example of a rock (Gabbro) whose two main constituent minerals are Diopside (a Clinopyroxene) and Anorthite (a Feldspar), with different melting temperatures of ca. $T_{Di} = 1400^o$C and $T_{An} = 1560^o$C, respectively (Fig. 3). Frictional heat is produced at the sliding interface, and diffuses into the rock, creating a temperature gradient with a series of isotherms roughly parallel to the fault. The melt boundary, by definition at the melting temperature, will follow to the first order either the isotherm 1400^o or 1560^{o}C depending on which mineral it crosses, forming an irregular profile with fluctuations at the scale of the mineral grains. In Fig. (3), a simplified sketch shows an idealization of such melting profiles for a bi-mineral rock under (a) a steep temperature gradient and (b) a gentle temperature gradient, showing that the topography of the interface is smaller under a steeper temperature gradient (Fig 4c-d). **This sketch is a simplification and idealization**

of the actual process, since isotherms in reality will be curved and other effects will play a role other than differences in melting temperature, such as variations in thermal conductivity or preferential melting in the vicinity of microcracks and mineral joints.

2.24 As shown in Nielsen et al. (2008), the thermal profile can be obtained by solving the Stefan problem with a migrating boundary. The temperature gradient will change (1) as a function of time, until at some point a steady-state condition is reached, and (2) as a function of the normal stress σ_n and slip rate V conditions, generating variable heat production rates $\tau V = f(\sigma_n, V, ...)$. The gradient is generally steeper at the beginning of sliding, because the penetration depth of thermal diffusion is bound, at the start, by $z \approx \sqrt{\kappa t}$, where κ is heat diffusivity. This is compatible with the observation of Hirose & Shimamoto (2005), who studied melting surfaces from high velocity slip experiments which were arrested at different stages of evolution from early melting to steady-state. They show how the melting surface evolved from a quite smooth topography in the early stages toward a rougher state. The temperature gradient is also steeper for conditions of high τV (e.g., under high slip-rate and normal stress), because the shortening rate ν (or velocity of the melting front advancement) is faster and the thermal boundary layer is bound, at later stages, by $z \approx \kappa/\nu$ (Nielsen et al., 2008).

2.25 Under steeper gradients the spacing between the two isotherms (1400 and 1560°C) is reduced and so is the offset of the thermal boundary layer when crossing different minerals. **Faults are rough at all scales but here we are primarily interested in the small-scale oscillations of the boundary between the melt and the solid host rock on either one side of the fault vein .** Therefore, to the first order we may equate such oscillations $z^{\pm}$ of the boundary due to a difference ΔT (for example, between Diopside and Enstatite) in melting temperature as:

2.26

$$\Delta T = T_{An} - T_{Di} \approx -2 \left.\frac{\partial T}{\partial z}\right|_{0^+} z^{\pm} \tag{10}$$

Assuming that the topography at the scale of interest is primarily shaped by the process of preferential melting, we may write $\omega_0 \approx z^{\pm}$:

2.27

$$\omega_0 \approx z^{\pm} \approx -\frac{1}{2}\Delta T \Big/ \left.\frac{\partial T}{\partial z}\right|_{0^+} \tag{11}$$

Solution of the Stefan problem under the steady-state (Eqs. 11 and 15, Nielsen et al. 2008) gives an estimate of temperature gradient

2.28

$$\partial T/\partial z|_+ \approx -\frac{1}{2}\,\tau_{ss}\,V\,(T_m - T_i)/[\kappa\,\rho\,(L + c(T_m - T_i))]. \qquad (12)$$

(see parameter defintion in Tab. 1), which we can combine with equation (11) in order to obtain the penetration depth (topography elevation) such that:

2.29

$$\omega_0 \approx \frac{2\,\Delta T}{\tau\,V}\,\frac{\kappa\,\rho\,(L + c(T_m - T_i))}{(T_m - T_i)} \qquad (13)$$

Hence the value of ω_0 should vary dynamically, depending on the heat production rate $\tau\,V$ and the way it affects the temperature gradient. We can make a theoretical prediction based on Eq. (13) for two experiments on gabbro where the heat production rate was measured: in experiment HVR726 (Fig 4-a) the imposed normal stress was $\sigma_n = 1.5\,\mathrm{MPa}$ and slip rate $V = 1.31\,\mathrm{m/s}$; a steady-state shear stress resistance of $\tau_{ss} = 0.81\,\mathrm{MPa}$ was measured, yielding a frictional heating rate $\tau_{ss}\,V \approx 1\,\mathrm{MW/m^{-2}}$ at the sliding interface. In experiment HVR687 (Fig 4-b) the conditions were $\sigma_n = 15.5\,\mathrm{MPa}$, $V = 1.14\,\mathrm{m/s}$ and $\tau_{ss} = 2.65\,\mathrm{MPa}$, yielding $\tau_{ss}\,V \approx 3\,\mathrm{MW/m^{-2}}$. Using Eq. (13) with gabbro parameters (Tab. 1) and an indicative value for average melting temperature fluctuations $\Delta T = 50^o\mathrm{C}$ (a smaller temperature difference than in the simplified anorthite/diopside example of Fig. 3), we predict $\omega_0 = 0.129\,\mathrm{mm}$ (HVR726) and $\omega_0 = 0.059\,\mathrm{mm}$ (HVR687) for dominant surface elevation in each experiment. These ω_0 values are fairly compatible with roughness measurements made by microscopic inspection directly on the samples, see below in section 3.

2.30 In addition, it is likely that the characteristic radius λ of the asperities is linked to ω_0, because (1) the size of the inhomogeneity sampled by the temperature fluctuation should increase with increasing penetration depth of the heat wave (2) preferential melting at grain boundaries and at sharp corners tends to eliminate isolated asperities and pronounced topographies with high curvature. This is illustrated by the ideal sketch in Fig. (3-b,c). In our model, for simplicity, we take the assumption that:

2.31

$$\omega_0/\lambda \approx \mathrm{Const} \approx 1 \qquad (14)$$

which will appear reasonable in the light of the experimental measures discussed below. As a consequence λ can be eliminated from Eq. (8) and the value of α may be simplified as follows:

2.32

$$\alpha \approx \sqrt{\frac{1}{2\pi}}\,\frac{\omega_0^2}{\omega^2}\,\exp\left(-\frac{\omega^2}{2\,\omega_0^2}\right) \tag{15}$$

2.33 This rule of thumb seems to be confirmed upon a preliminary inspection of thin sections of Gabbro samples where experimental conditions led to different melting rates and temperature gradients during high velocity slip (see below).

3 Observations on natural and experimental samples

3.34 We obtain an independent estimate of both half-variance (i.e. ω_0) and dominant radius (i.e. λ), by performing a quantitative analysis of the digital profiles from several experiments (Tab. 2). We use a method originally proposed by Yamada et al. (1978) in order to describe roughness of dry frictional surfaces, henceforth implemented by Yoshioka & Scholz (1989) in order to model the shear stiffness and normal closure of contacting solids. It is assumed for these measurements that the profile can be satisfactorily represented as a population of spherical asperities. A characteristic height ω_0 is defined as the root mean square of the probability density function $\psi(z)$ of the asperity elevation z with respect to a reference line, and λ is defined as the average radius of curvature in a population of spherical caps fitting the individual asperity summits (see Fig. 1 and caption text for further details).

3.35 **The resulting measurements performed on posthumus slip surfaces are shown in Tab. (2) and Fig. (5). Within the resolution of this qualitative fit, we find for the five experimental gabbro samples (1) a strong correlation in the variations of λ and ω_0 (see Fig. 5-a), confirming that both values vary in unison and (2) that the roughness elevation decreases under steeper temperature gradients (see Fig. 5-b) as expected from the discussion on preferential melting and Fig. (3). The values of $\omega_0 = 0.124\,$mm and $\omega_0 = 0.069\,$mm obtained for experiments HVR726 and HVR687 (Tab. 2) are consistent with the estimates obtained in the previous paragraph using Eq. (13) and $\Delta T = 50^o\,$C. These preliminary results seem to corroborate the theoretical arguments leading to Eqs. (11) and (14). In Fig. (5) a graphical synthesis of the measurments is presented, showing the correlation**

of ω_0, λ and their variation with the heat production rate in comparison to the theoretical prediction of Eq. (13).

3.36 In order to compare the measurements obtained from our experimental samples to similar occurrences on natural faults (under arguably similar conditions and settings), we performed the same surface measurements on a sample from ancient seismic faults of the Gole Larghe fault zone, Italian Alps (Di Toro & Pennacchioni, 2004). The sample SEM image and the profile used for the measurements are shown in Fig. (6). Since the host rock (tonalite) in this case is quite different from the gabbro samples used in the experiments, we also performed for reference measurements on sample HVR376 (Tab. 2), retrieved from an experiment which was performed on tonalite from the same outcrop as L05_06. It appears that there is a substantial decrease in both λ and ω_o when comparing the experimental results of HVR376 performed at $\tau_{ss} V \approx 5\,\mathrm{MW\ m^{-2}}$ to the natural fault sample L05_06 where the estimated work rate is much higher ($30 < \tau_{ss} V < 107\,\mathrm{MW\ m^{-2}}$). It should be stressed that this single sample is shown only as an example of possible situation on natural pseudotachylite-bearing fault. The measure is indicative and not sufficient as supporting evidence that our melting roughness hypothesis holds true under natural conditions. As custumary, we leave for future studies the endeavour of obtaining and analysing a sufficient number of field and experimental data to perform a significant test of the present theory.

3.37 While the measures are straightforwardly obtained from experimental samples and lead to consistent results, those performed on natural faults are more thorny. First, the fossil fault structure and thickness are highly variable along strike: extension jogs that cumulate abundant solidified melt are interspersed within thin fault veins and contraction bends, as commented in the introduction. The locally thicker melt pools do not sustain significant friction, so that the thinner areas only are representative of the rupture dynamics. As a consequence, one should select a sample within one of the thin fault segments in order to obtain a representative characterization of the sufrace. Second, if the fault has cumulated slip in the order tens of cm or more, the two sides of the fault finally facing each other (in the observed position) may have been generated on rather different segments

of the fault and withstood distinct conditions of thickness and normal stress before they became adjacent. It follows that the two opposing melting boundaries on each side of the melt can have a contrasting surface structure in terms of roughness, preferential melting and the parameters ω_0 and λ. While the experimental samples are rather symmetric and homogeneous, natural faults show a highly variable and asymmetric structure of the pseudotachylite vein. In the example of sample shown here from a natural fault (L_05_06 in Fig 6) there is a clear difference between the bottom and the top profiles (the top profile shows a relatively accentuated topography with larger ω_0 with respect to the extremely flat bottom one). In conclusion, an accurate study of a natural pseudotachylite-bearing fault may require several measurements along different spots of the fault in order to obtain a good coverage of the variability.

4 Normal stress and melt thickening

4.38 To sum-up, we introduced partial contact at asperities under state incipient yield, and assumed that the melt/solid boundary has a topography of dominant elevation ω_0 and wavelength λ. We argued that both ω_0 and λ are dynamically determined, related to the temperature gradient and that they vary in concert such that $\omega_0/\lambda \propto$ const. The residual stress resulting from the contact asperities is $\alpha\,\sigma_c$, where α increases when $\omega \to \omega_0$. We now recall the main equations that we obtained to describe the normal stress:

4.39

$$\begin{aligned} \sigma_n &= (1-\alpha)\,\tfrac{C\,\eta_e\,\dot{\omega}_c\,R^2}{\omega^3} + \alpha\,\sigma_c \quad \text{(a)} \\ \alpha &= \sqrt{\tfrac{1}{2\pi}}\,\tfrac{\omega_0^2}{\omega^2}\,e^{-\frac{\omega^2}{2\,\omega_0^2}} \quad \text{(b)} \\ \omega_0 &\approx z^{\pm} \approx \tfrac{1}{2}\Delta T \Big/ \left.\tfrac{\partial T}{\partial z}\right|_{0+} \quad \text{(c)} \end{aligned} \tag{16}$$

(with the constraint that $\alpha(\omega) \leq \sigma_n/\sigma_c$).

4.40 From Eq. (16-a) we may derive the squeezing (extrusion) rate $\dot{\omega}_c$. Note that in the particular case of steady-state conditions, the thickness of melt is constant, therefore squeezing rate can be equated to rate of melting: $\dot{\omega}_c = \nu$ (extrusion exactly compensates melt production, where ν is the rate of melting or the velocity of advancement of the melting front into the solid). However in the transient regime, the thickness does vary so that we need to estimate its

evolution based on a balance between extruded volume and melted volume. As a consequence, we may write at any time t the differential equation defining the rate of thickening, and its time integration (or its discrete approximation) yielding the thickness evolution:

4.41

$$\begin{aligned} \dot{\omega}(t) &= -\mathrm{H}\left(\dot{\omega}_c(t)\right) + \nu(t) \quad \text{(a)} \\ \omega(t) &= \int_0^t \dot{\omega}(t)\, dt' \quad \text{(b)} \end{aligned} \tag{17}$$

where $\dot{\omega}$ refers to the time derivative of the average melt thickness while $\dot{\omega}_c$ refers to the rate of squeezing only, and ν to the melting rate. The convergence due to squeezing should always be positive, since we assume that once extruded the melt cannot be sucked in again; this is why we introduce the Heaviside step function H. On the other hand, melting rate ν can be reversed in a freezing rate and thus may take both positive and negative values.

4.42 In order to complete the solution of the equation system (16) the melting rate ν and the temperature gradient $\frac{\partial T}{\partial z}|_{0^+}$ are computed by solving the Stefan problem of migrating boundary. In the transient regime, it is necessary to perform a numerical solution, which will be the topic of future work (Nielsen et al., submitted to *Jour. Geophys. Res.*, 2010). However, the analytical solution is straightforward if the steady-state condition is assumed as proposed by (Nielsen et al., 2008). Such solution is the object of next section.

5 Improved steady-state solution

5.43 From (Nielsen et al., 2008, Eqs. 11, 15, 36), we may write:

$$\begin{aligned} \nu &= \frac{\tau_{ss} V}{2\rho(L + c(T_m - T_i))} \quad \text{(a)} \\ \frac{\partial T}{\partial z}|_{0^+} &= \frac{\nu}{\kappa}(T_m - T_i) \quad \text{(b)} \\ \omega &= \frac{W \eta_c}{2\tau_{ss}} \frac{\operatorname{atanh}\left(\frac{V/W}{\sqrt{1+V^2/W^2}}\right)}{\sqrt{1+V^2/W^2}} \quad \text{(c)} \end{aligned} \tag{18}$$

where η_c and W are constitutive parameters (see Tab. 1) governing the viscosity temperature dependence, T_m and T_i is the average melting temperature of the rock and initial temperature, respectively. We recall that frictional melt experiments (Hirose & Shimamoto, 2005; Del Gaudio et al., 2009) show a transient evolution of shear stress with ongoing slip followed by a stable value τ_{ss}, attesting the onset of a steady-state condition. The steady-state is reached because melt extrusion balances the heat production (Nielsen et al., 2008). By substituting the Eqs.

(18) into Eqs. (16-b, c), we may write the ratio ω_0/ω and find that all variables except slip rate V simplify and the ratio depends on constitutive parameters of the rock only:

$$\left(\frac{\omega_0}{\omega}\right)_{ss} = \frac{2\,\kappa\,\rho\,(L + c\,(T_m - T_i))\,\sqrt{1 + \frac{V^2}{W^2}}\Delta T}{(T_m - T_i)\,V\,W\,\eta_c\,\mathrm{atanh}\left(\frac{V/W}{\sqrt{1+\frac{V^2}{W^2}}}\right)} \tag{19}$$

5.44 As a consequence $\alpha(V) = (1/\sqrt{2\pi})\,(\omega_0^2/\omega^2)\,e^{-\frac{\omega^2}{2\omega_0^2}}$, the ratio of contact asperities to total area during frictional melt steady-state conditions, depends on slip velocity alone. This is a striking result, which can be interpreted on the basis that both ω and ω_0 are inversely proportional to the steady-state shear stress τ_{ss} which factors out, while the effective melt viscosity (indirectly controlling melt thickness through the heat balance of the system), depends on slip rate alone (Eq. 42 in Nielsen et al., 2008). Thus ratio of thickness to roughness may allow to estimate slip-rate during past earthquakes in natural fossil faults bearing pseudotachylite, assuming that the final fault sliding occurred close to a steady-state condition. This point is discussed more in detail in next section.

5.45 In addition, in agreement with (Nielsen et al., 2008 Eqs. 42, 51) we may use the following expressions :

5.46

$$\eta_e = \frac{W\,\eta_c\,\mathrm{atanh}\left(\frac{V}{W\sqrt{\frac{V^2}{W^2}+1}}\right)}{3\,V\,\sqrt{\frac{V^2}{W^2}+1}} \tag{20}$$

$$\tau_{ss} = \frac{V\,\eta_e}{6\,\omega} \tag{21}$$

which, in conjunction with Eq. (16-a) yield a fourth order polynomial expression in τ_{ss}. There is only one positive, real root of such a polynomial, resulting in the steady-state shear stress:

5.47

$$\tau_{ss} = A\left(\frac{\sigma_n - \alpha_{ss}(V)\,\sigma_c}{1 - \alpha_{ss}(V)}\right)^{1/4} \frac{\sqrt{\mathrm{atanh}(\frac{V/W}{\sqrt{1+V^2/W^2}})}}{(1 + V^2/W^2)^{1/4}} \tag{22}$$

5.48

$$\text{where} \quad A = \frac{\sqrt{W\,\eta_c/R}}{3\sqrt{2}}\left(\frac{\rho\,(L + c\,(T_m - T_i))}{3\,C}\right)^{1/4}$$

The value of $\alpha_{ss}(V)$ is computed according to Eqs. (16-b, 19). As $\alpha_{ss}(V)$ varies with slip rate, an important consequence is that the dependence of friction on normal stress σ_n on one side, and on slip velocity V on the other, are not decoupled. This is a remarkable difference with the approximate frictional form proposed in (Nielsen et al., 2008). The latter frictional form is a good approximation of the one proposed here at relatively high slip rate. Indeed the coefficient α becomes negligible at high slip rates and the normal stress dependence identical to that of (Nielsen et al., 2008) is retrieved.

5.49 **[I-2] Due to the rough and irregular shape of the melt boundaries the assumption of laminar flow across the melt is questionable. The approximation holds provided that the lubricant thickness is small compared to the wavelength of the roughness (Brodsky & Kanamori, 2001); however here both lengths fall in the same order of magnitude. As a consequence we expect the development of turbulence and mixing to some extent, depending on the particular combination of boundary roughness and Reynolds number. In this context equations (18,20,21) should be considered as an effective medium approximation of practical use (a common practice in fluid dynamics for problems involving turbulence, see for example Goldstein, 1938). The small scale turbulence is ignored but effective parameters such as η_c and W implicitly account for the increase of apparent viscosity (by transfer of momentum by eddies) and increase in diffusivity (by local transport and mixing). In Nielsen et al (2008) η_c and W are retrieved by empirical fit of experimental data.**

5.50 We show examples of friction at the steady-state as a function of normal stress, slip velocity and both (Figs. 7,8). **Since the ratio of shear stress to normal stress is not constant under lubricating conditions, the very definition of a friction coefficient is awkward and we rather represent the results in terms of absolute friction.** We used constitutive parameters compatible with a gabbro (see Tab. 1); the geometry corresponds to that a cylindrical sample of 1 cm ($R = 10^{-2}$ m, C=3/16); we set $\Delta T = 80^o$C to model the differential melting and $\eta_c = 7.5\,10^3$ Pa s, $W = 0.21$ m/s for the Arrhenious equivalent-viscosity law according to Nielsen et al. (2008).

6 Relating slip rate V and ω/ω_0

6.51 A back-of the envelope rationale for Eq. (19) is the following. As argued above, the roughness ω_0 is strongly related to inhomogeneous melting temperatures and hence scales with the temperature gradient (Eq. 16-c).

6.52 On the other hand, as shown in (Nielsen et al., 2008), the temperature gradient is proportional to melt front advancement velocity, which is driven by the heat rate production or τV (at least under conditions reasonably close to the steady-state). In addition, the resulting friction can be described as viscous shear upon definition of an equivalent viscosity η_s across the melt layer.

6.53 We may express in simplified equations the above arguments, such that:

$$\begin{aligned} \omega_0 &\propto 1/(\partial T/\partial z)_{0^+} \\ \partial T/\partial z|_{0^+} &\propto \nu \propto \tau V \\ \tau &= \eta_s V/2\,\omega \end{aligned} \tag{23}$$

which may be combined into:

6.54

$$\omega/\omega_0 \propto \eta_s(V)\,V^2. \tag{24}$$

Finally, assuming a linearized Arrhenious law, an expression for the equivalent viscosity η_s can be derived (Nielsen et al., 2008). The latter shows a negative slip-rate dependence which may be roughly approximated by $\eta_s \propto 1/V$ at high slip rates, yielding:

$$\omega/\omega_0 \approx \frac{1}{a}\,V \tag{25}$$

6.55 The characteristic velocity a may be estimated based on laboratory tests at different velocities for a given rock type. For gabbro, based on the experiments of (Fig. 4-e), we obtain an indicative value $a \approx 2.5 \pm 0.7$m/s (for HVR726, the final sliding velocities were $V = 1.31\,\mathrm{m/s}$ and we measure $\omega_0 = 0.236$ and $\omega = 0.22$mm; for HVR687, $V = 1.14\,\mathrm{m/s}$, $\omega_0 = 0.08$ and $\omega = 0.22$mm).

6.56 Ideally, Eq. (25) may be used to estimate V independently of τ and other ambient conditions by inspection of fossil fault samples. However as commented at the end of section

2, the structure of a natural fault is highly non symmetric and variable along strike so that an accurate characterization may require multiple samples and measures along fault strike.

Conclusions

6.57 We include the effect of partial asperity contact across the melt layer, on order to obtain a theoretical prediction of rock friction in the presence of melting. The normal stress is supported in part at contact asperities and in part by the pressure of the viscous melt layer, and this affects the resulting friction across the fault in a non-linear fashion.

6.58 We show that at the small scale, the roughness of the melting surface does vary depending on the sliding conditions, and can be linked to the temperature gradient into the side walls of the fault. As a consequence, the amount of partial contact area α, and the partitioning of normal stress, generally depend on sliding conditions.

6.59 We quantify the above arguments and incorporate them into the expression for steady-state friction in the presence of melt. In the resulting friction law, the effect of normal stress and the effect of slip-rate are coupled through the contact ratio coefficient α.

6.60 Finally, we show that the ratio of roughness ω_0 (defined as the rms of the probability density distribution of asperity elevation) and the average melt thickness ω only depend on sliding velocity, so that ω/ω_0 could ideally be used as a gage to estimate past slip-rates on fossil earthquake faults.

Acknowledgements

We acknowledge Takehiro Hirose for providing sample HVR 687. Stefan Nielsen was granted by the MIUR project FUMO, and Giulio Di Toro and Stefan Nielsen were granted by the European Research Council Starting Grant Project 205175 (USEMS) and CA.RI.PA.RO. We thank Leonardo Tauro for thin section preparation, Luca Peruzzo, Steven Smith and Piergiorgio Scarlato for SEM facilities and Toshi Shimamoto for his constant support. Finally, we are grateful to Nick Beeler and Chris Marone for their constructive reviews.

References

Beeler, N., Tullis, T., & Goldsby, D., 2008. Constitutive relationships and physical basis of fault strength due to flash heating, *J. Geophys. Res.*, **113**(B1), B01401.

Bizzarri, A. & Cocco, M., 2006. A thermal pressurization model for the spontaneous dynamic rupture propagation on a three-dimensional fault: 1. methodological approach, *J. Geophys. Res.*, **111**, B05303.

Brantut, N., Schubnel, A., Rouzaud, J., Brunet, F., & Shimamoto, T., 2008. High velocity frictional properties of a natural clay bearing fault gouge, *J. Geophys. Res.*, **113**, B10401.

Brodsky, E. & Kanamori, H., 2001. The elastohydrodynamic lubrication of faults, *J. Geophys. Res.*, **106**(B8), 16357–16374.

Del Gaudio, P., Di Toro, G., Han, R., Hirose, T., Nielsen, S., Shimamoto, T., & Cavallo, A., 2009. Frictional melting of peridotite and seismic slip, *J. Geophys. Res.*, **114**, B06306.

Di Toro, G. & Pennacchioni, G., 2004. Superheated friction-induced melts in zoned pseudotachylytes within the adamello tonalites (italian southern alps), *J. Struct. Geol.*, **26**, 1783–1801.

Di Toro, G., Goldsby, D., & Tullis, T., 2004. Friction falls towards zero in quartz rock as slip velocity approaches seismic rates, *Nature*, **427**, 436–439.

Di Toro, G., Nielsen, S., & Pennacchioni, G., 2005. Earthquake rupture dynamics frozen in exhumed ancient faults, *Nature*, **436**, 1009–1012.

Di Toro, G., Pennacchioni, G., & Teza, G., 2005. Can Pseudotachylyte be used to infer earthquake source parameters? An example of limitations in the study if exhumed faults, *Tectonophysics*, **402**, 3–20.

Di Toro, G., Hirose, T., Nielsen, S., Pennacchioni, G., & Shimamoto, T., 2006. Natural and experimental evidence of melt lubrication of faults during earthquakes, *Science*, **311**, 647–649.

Dieterich, J. H. & Kilgore, B., 1994. Direct observation of frictional contacts; new insights for state-dependent properties, *Pure Appl. Geophys.*, **143**, 283–302.

Fialko, Y. & Khazan, Y., 2005. Fusion by earthquake fault friction: Stick or slip?, *J. Geophys. Res.*, **110**, B12407.

Goldsby, D. L. & Tullis, T. E., 2002. Low frictional strength of quartz rocks at subseismic slip rates, *Geophys. Res. Lett.*, **29**, L01240.

Goldstein, S., 1938. *Modern Developments in Fluid Dynamics*, Oxford University Press, Fluid Motion Panel of the Aeronautical Research Committee and Others.

Greenwood, J., 1992. Contact of rough surfaces, in *Fundamentals of friciont: macroscopic and microscopic processes*, edited by I. Singer & H. Pollock, Kluwer, Dordrecht.

Hamada, Y., Hirono, T., Tanikawa, W., Soh, W., & Song, S.-R., 2009. Energy taken up by co-seismic chemical reactions during a large earthquake: An example from the 1999 taiwan chi-chi earthquake, *Geophys. Res. Lett.*, **36**, L06301.

Han, R., Shimamoto, T., Hirose, T., Ree, J.-H., & Ando, J., 2007. Ultralow friction of carbonate faults caused by thermal decomposition, *Science*, **316**, 878–881.

Hirono, T., Yokoyama, T., Hamada, Y., Tanikawa, W., Mishima, T., Ikehara, M., Famin, V., Tanimizu, M., Lin, W., Soh, W., & Song, S., 2007. A chemical kinetic approach to estimate dynamic shear stress during the 1999 taiwan chichi earthquake, *Geophys. Res. Lett.*, **34**, L19308.

Hirose, T. & Shimamoto, T., 2003. Fractal dimension of molten surfaces as a possible parameter to infer the slip-weakening distance of faults from natural pseudotachylytes, *Journal of Structural Geology*, **25**, 1569–1574.

Hirose, T. & Shimamoto, T., 2005. Growth of molten zone as a mechanicsm of slip weakening of simulated faults in gabbro during frictional melting, *J. Geophys. Res.*, **110**, B05202.

Jeffreys, H., 1942. On the mechanics of faulting, *Geological Magazine*, **79**, 291–295.

Landau, L. & Lifshitz, E., 1975. *Theory of Elasticity*, Pergamon, New York.

Lee, J. & Ladd, A., 2002. A computer simulation study of multiphase squeezing flows, *Physics of fluids*, **14**, 1631–1641.

Nielsen, S., Di Toro, G., Hirose, T., & Shimamoto, T., 2008. Frictional melt and seismic slip, *J. Geophys. Res.*, **113**, B01308.

Persson, B., 2000. *Sliding Friction, Physical Principles and Applications*, Springer-Verlag, New York.

Pittarello, L., Toro, G. D., Bizzarri, A., Pennacchioni, G., Hadizadeh, J., & Cocco, M., 2008. Energy partitioning during seismic slip in pseudotachylyte-bearing faults (gole larghe fault, adamello, italy), *Earth and Planetary Science Letters*, **269**, 131–139.

Rice, J. R., 2006. Heating and weakening of faults during earthquake slip, *J. Geophys. Res.*, **111**, B05311.

Scholz, C. H., 1990. *The mechanics of earthquakes and faulting*, Cambridge University Press.

Shand, 1916. The pseudotachylyte of parijs (orange free state) and its relation to trapp-shotten gneiss and flinty crush rock, *Quart. J. Geol. Soc. London,*, **72**, 198–221.

Sibson, R., 1975. Generation of pseudotachylyte by ancient seismic faulting, *Geophys. J. R. Astron. Soc.*, **43**, 775–794.

Spray, J., 1992. A physical basis for the frictional melting of some rock forming minerals, *Tectonophysics*, **204**, 205–221.

Spray, J., 1995. Pseudotachylyte controversy; fact or friction?, *Geology*, **23**, 1119–1122.

Spray, J. G., 2005. Evidence for melt lubrication during large earthquakes, *Geophys. Res. Lett.*, **32**, L07301.

Sulem, J. & Famin, V., 2009. Thermal decomposition of carbonates in fault zones: Slipweakening and temperature limiting effects, *J. Geophys. Res.*, **114**, B03309.

Tsutsumi, A. & Shimamoto, T., 1997. High-velocity frictional properties of gabbro, *Geophys. Res. Lett.*, **24**, pp.699–702.

Yamada, K., Takeda, N., Kagami, J., & Naoi, T., 1978. Surface density of asperities and real distribution of asperity heights on rubbed surfaces, *Wear*, **47**, 5–20.

Yoshioka, N. & Scholz, C., 1989. Elastic preoperties of contacting surfaces under normal and shear loads 1. theory, *J. Geophys. Res.*, **94**(B12), 17691–17700.

Tables, Figures and captions

		gabbro:
ρ	mass density	3000 kg / m^3
κ	thermal diffusivity	$0.48\,10^{-6}$m^2/ s
c	heat capacity	950 J / kg ^{o}C
L	latent heat	350 10^3J / kg
ΔT	temperature difference (preferential melting)	-
T_m, T_i	melting and initial temperatures	1200, 20^{o}C
R	extrusion radius of melt patch	-
σ_n	normal stress	-
τ, τ_{ss}	shear stress, general and steady-state, resp.	-
ν	shortening rate	-
$\dot{\omega}_c$	extrusion rate	-
V	slip rate	-
W	characteristic velocity used in viscosity law	0.21 m/s
η_c	characteristic viscosity used in viscosity law	7.5 10^3Pa s
η_e, η_s	equivalent viscosities (for shear and extrusion, resp.)	-
ω	half thickness of melt layer	-
ω_o	characteristic height of asperities	-
λ	characteristic radius of asperities	-
$\psi(z)$	probability density function of asperity heights	-
α, α_{ss}	ratio of contact asperities to total area	-
σ_c	indentation yield strength	150 10^6Pa

Table 1: Main parameters and variables defined. MKS units are assumed unless otherwise specified (for ease of reading mm and MPa are used as specified in some text and figures).

.

sample nr.	rock type	λ (mm)	ω_0 (mm)	$\tau_{ss} V$ (MW/m^2)
HVR687	gabbro	0.063±0.028	0.069±0.017	3.00±0.15
HVR688	”	0.134±0.031	0.079±0.002	1.51±0.07
HVR726	”	0.191±0.016	0.124±0.007	1.06±0.05
HVR737	”	0.095±0.006	0.100±0.002	1.02±0.05
HVR376	tonalite	0.116±0.027	0.109±0.003	5.02±0.15
L05_06$^{(*)}$	tonalite nat.	0.087±0.008	0.0296±0.0143	32–107$^{(**)}$

$^{(*)}$ sample from natural fault.

$^{(**)}$ estimated from the amount of pseudotachylite and offset.

Table 2: Measures from experimental and natural faults describing topography of melt/solid boundaries, melt thickness and slip conditions. λ is average radius of spherical apserity caps, ω_0 is the characteristic elevation of the asperities on the surface (e.g., the rms of the asperity height probability distribution), ω is the average thickness of melt and τV is the average power developed during dynamic slip (the product of average shear stress and slip rate). τV is measured for all the HVR experiments but inferred for the fossil fault outcrop L05_06 according to the method explained in Di Toro et al. (2006), using the field observations on amount of pseudotachylite (an average of about 7 mm including veins and pools) and measured offset (ranging 0.3-1m, resulting in the large span of τV).

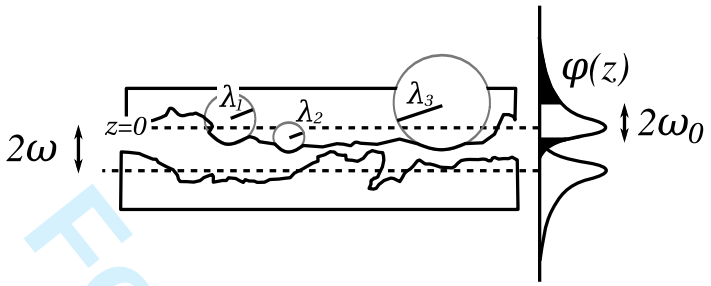

Figure 1: We Illustrate the meaning of ω, ω_0 and λ in the equations. $\psi(z)$ is the probability density function of the asperity heights with respect to a reference line (dotted line). Note that the dotted line ($z = 0$) does not in general co" ncide with the peak of the elevation density distribution $\psi(z)$ (unless ψ is symmetric which is usually not the case), but rather with the average value. Since the intersticial space is filled with melt (more precisely a viscous body composed by melt with clasts in suspension), 2ω is defined as the average thickness of the melt. For the characterization of a sample surface, at each local maximum in the topography the local curvature is measured and the asperity summit is modeled as a spherical cap of radius λ_n(an arc of circle in the 2D section). For sake of clarity, only three such spheres are represented. Finally, ω_0 is defined as the rms of distribution $\psi(z)$ and λ as the average radius in the distribution of the spherical caps fitting individual asperities.

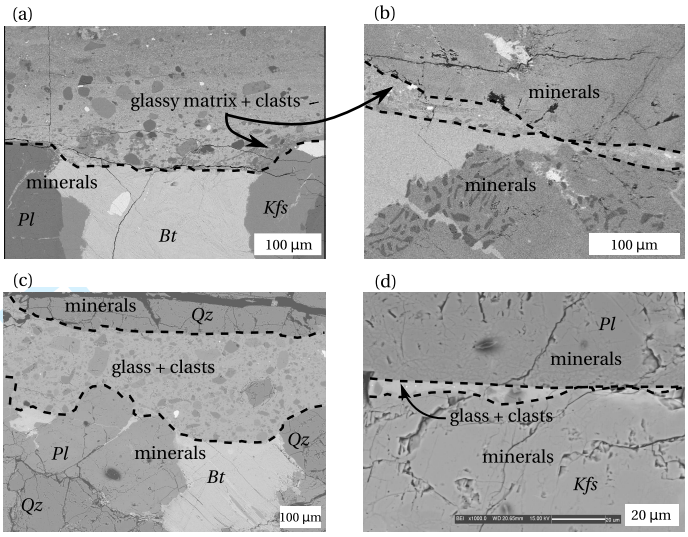

Figure 2: Back Scatter Electron Microscope images of natural and experimental pseudotachylites (glass or glassy cryptocrystalline matrix from solidified melt with mineral clasts) hosted in granitoid rocks (Tonalite). (a,b) Natural ancient fault from the Gole Larghe Fault zone, (Italian Alps, Di Toro et al. (2006)). (c,d) Experimental fault from high velocity rock friction experiments performed on the same host granitoids as (a). In (b) and (d) details are shown where the glassy layer is extremely thin and the minerals are in contact across an asperity. Pl: Plagioclase (melting point 1200^{o}C); Bt: Biotite (melting point 650^{o}C); Kfs: K-Feldspar (melting point 1150^{o}C); Qz: Quartz (melting point 1700^{o}C).

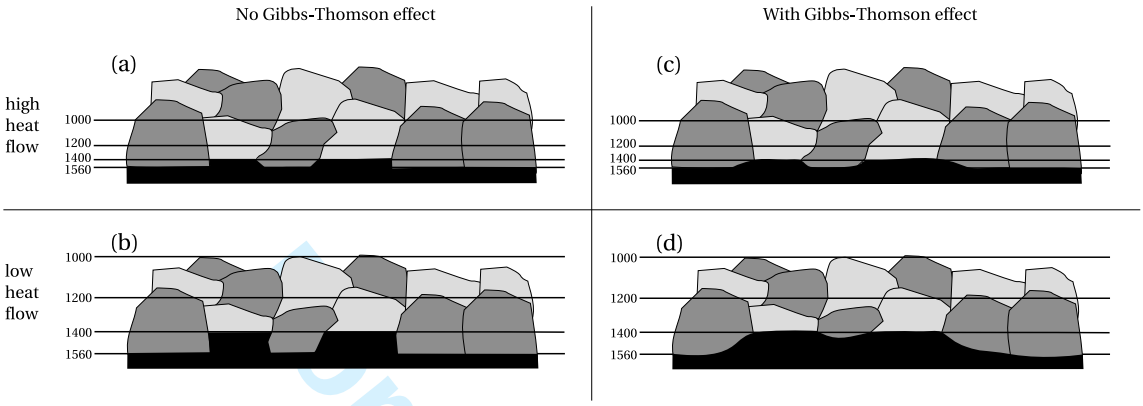

Figure 3: Idealized models of melting boundary in a 2 mineral rock. Dark grey areas represent minerals melting at relatively high temperature (e.g, Anorthite, 1560^{o}C), while lighter areas minerals with low melting temperature (e.g. Diopside, 1400^{o}C). Black areas represent melt. The straight lines show isocontours of temperature in the rock. (a,b): steep and gentle temperature gradient, resp., with melting boundary strictly following the isotherms in each mineral. (c,d): same temperature gradients as (a,b) but the melt/solid boundaries are drawn in a more round-shaped fashion to account for the preferential melting of sharp corners and isolated asperities. In (a,b) the temperature gradient affects the only the asperity height in the profile topography, which is smaller for the steeper gradient in (a), while in (c,d) it affects both the height and the asperity radius distribution. Higher heat flows are found either during the early phases of melting or under conditions of high normal stress and slip rate (see text for details).

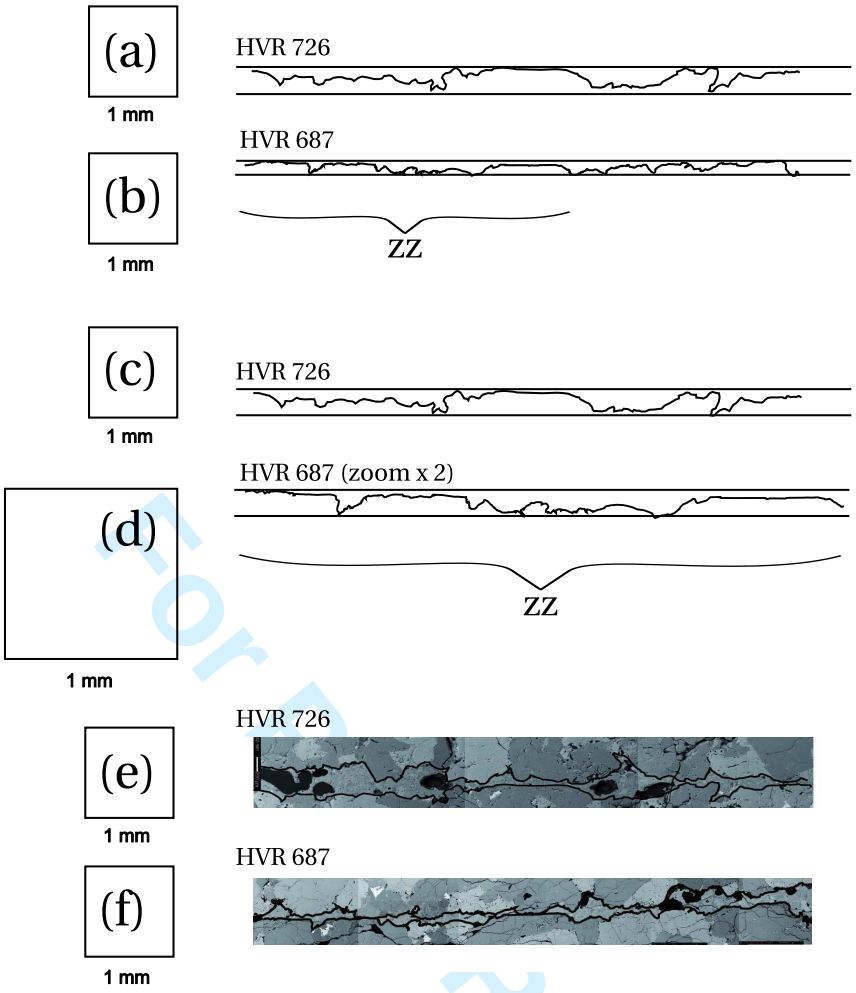

Figure 4: Profiles drawn from samples of experiments performed on Gabbro (37% Diopside, light grey, melting point 1400°C; 33% Anorthite, dark grey, melting point 1560°C; 30% other minerals). (a) HVR726 performed under$\sigma_n = 1.5\,\mathrm{MPa}$, $V = 1.31\,\mathrm{m/s}$, $\tau V \approx 1\,\mathrm{MW/m^{-2}}$ (i.e. low heat flow and gentle temperature gradient) and (b) HVR687 performed under $\sigma = 15.5\,\mathrm{MPa}$, $V = 1.14\,\mathrm{m/s}$, $\tau V \approx 3\,\mathrm{MW/m^{-2}}$ (i.e. high heat flow and steep temperature gradient). The profiles qualitatively show the same effect as in idealized models of Fig. (3) showing both wavelength and elevation effect, for conditions of gentle and steep temperature gradients, respectively. (c,d) show the same profiles, but with a zoom of a factor of 2 for HVR 687. Upon inspection, zooming in (d) produces a structure on a very similar sale as profile (a), illustrating a rescaling of both wavelength and elevation (λ, ω_0) in the profiles with the increase of temperature gradient. This rescaling is confirmed by a quantitative analysis of the elevation distribution as discussed in the text. (e) and (f) show photomozaics from BSE-SEM images of the original thin sections: the profiles are digitized from the bottom solid/melt boundaries (indicated by black curves) in both experiments.

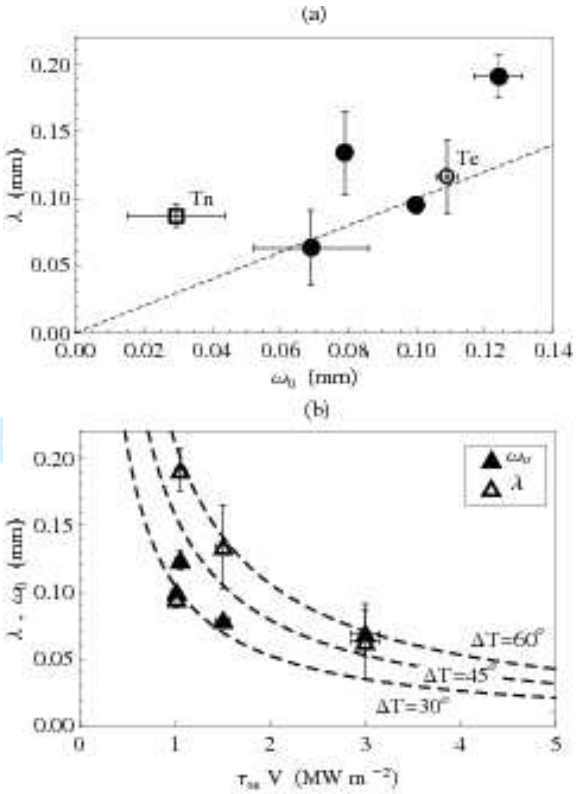

Figure 5: Characteristic asperity height ω_0 and radius λ, plotted (a) against each other and (b) as a function of the heat production rate $\tau_{ss} V$, for fault surfaces from experiments summarized in Tab. (2). (a) The curve $\lambda = \omega_0$ is shown in as a dashed line for reference. The square (marked Tn) represents the tonalite sample from the natural fault profile L05_06 of Fig. (6) and the circle marked Te represents experiment HVR376 performed on the same tonalite host rock. Black disks represent the gabbro experiments of Tab. (2). (b) The dotted curves show the theoretical penetration depth of isotherms $\Delta T = 30, 45, 60$°C according to Eq. (13) for reference, while the black and white triangles represent the measures of ω_o and λ, repsectively, from the experimental gabbro samples of Tab. (2).

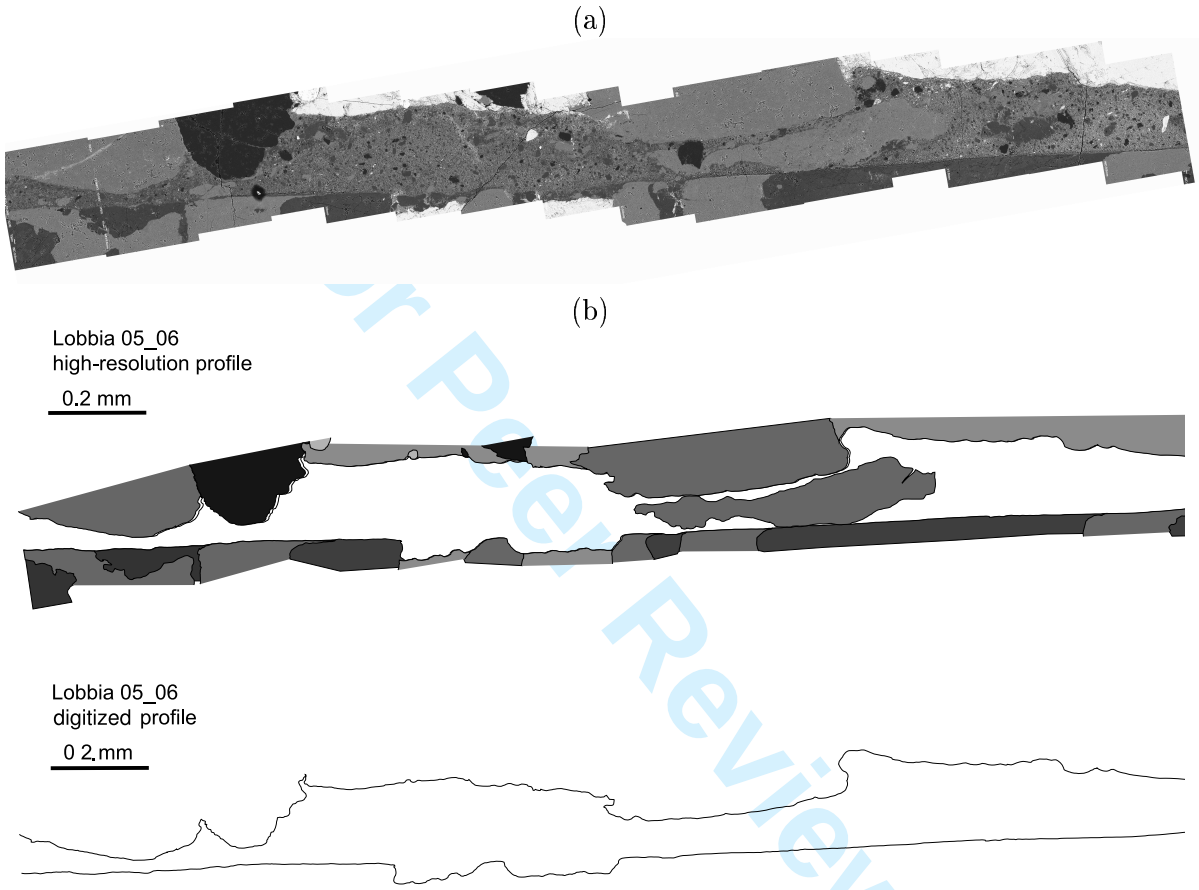

Figure 6: Fault vein profile from natural fault (Adamello, Trentino, Eastern Italian Alps). (a) SEM image, (b) mineral identification and redrawn high-resolution profile

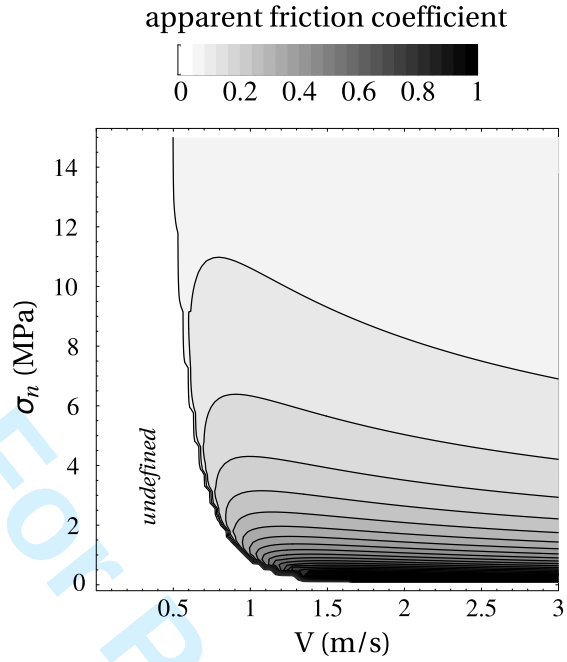

Figure 7: Apparent friction coefficient as a function of slip rate and normal stress. Undefined domain on the left corresponds to the unphysical case $\alpha_{ss}\sigma_c > \sigma_n$, yielding to an imaginary solution in Eq. (22). See text for more details.

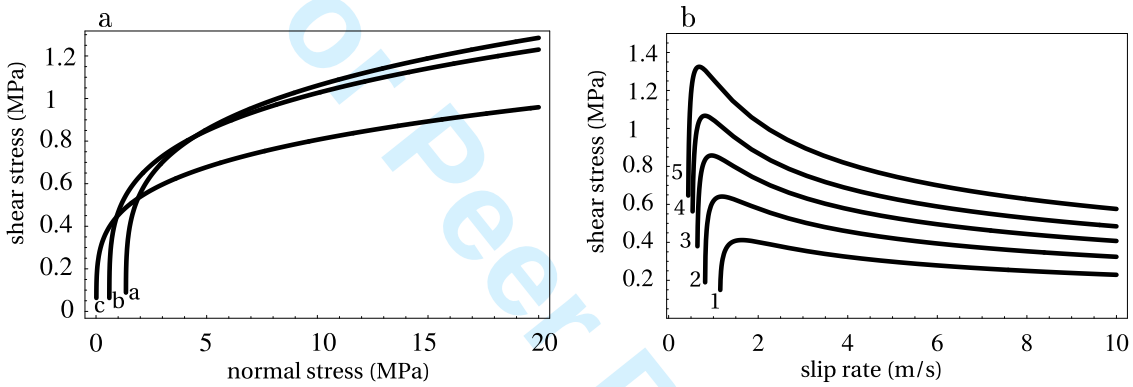

Figure 8: (a) Dependence of shear stress on normal stress, for three different slip rates (a, b, c are curves for $V = 0.9$, 1.1 and 2.5 m/s, resp.). (b) Dependence of shear stress on slip rate, for five different normal stresses (1, 2, 3, 4, 5 are curves for $\sigma_n = 0.5$, 2, 5, 10, 20 MPa, resp.)